THE ASTROPHYSICAL JOURNAL, 236:577–591, 1980 March 1

THE GALACTIC FOUNTAIN OF HIGH-VELOCITY CLOUDS

JOEL N. BREGMAN
Astronomy Department, Columbia University
Received 1979 May 7; accepted 1979 August 27

ABSTRACT

We examine whether high-velocity clouds of neutral hydrogen (not the Magellanic Stream), observed in every longitude quadrant of the sky, can condense from a hot, dynamic corona above the plane of the Galaxy. Supernova-heated gas that arises above the disk must either flow outward as a wind or remain bound to the Galaxy in a dynamic corona in which gas is constantly in motion—a static corona is not stable. Since clouds cannot condense in a wind, we favor a corona and show that it is consistent with current values for the supernova heating rate above the disk. Gas continuously entering the corona from the disk rises up (in Z) and outward (in ϖ) in an attempt to reach static equilibrium with the corona. The gas behaves adiabatically until radiative losses become important. Then, coronal gas is susceptible to thermal instabilities and neutral clouds condense from the corona. Clouds form toward the top of the corona at about one density scale height because thermal instabilities grow most rapidly there. After formation, clouds fall ballistically toward their point of origin.

To explain the observed cloud velocities, we argue that as coronal gas flows outward, it conserves its angular momentum. Then, the velocities of clouds from differential galactic rotation are much greater than normal differential rotational velocities (no outward motion of coronal gas before forming into clouds). Without pressure support, clouds plummet downward and radially inward, providing the velocities to clouds seen overhead and toward the anticenter, respectively. We demonstrate that gas must travel outward 2–3 times its original position and up to $Z \approx 5$–10 kpc before forming clouds. Also, the corona is nearly hydrostatic in Z. Because of a pressure gradient at the base of the corona, the hot gas flows radially outward; some clouds form in the outward flow. The dynamic corona is modeled with a two-dimensional hydrodynamic code that includes radiative cooling, rotation, and a mass model of the Galaxy with an extended halo. We reproduce the major velocity features of the high-velocity clouds without violating any observational or theoretical constraints if the density and temperature at the base of the corona above the Sun are $1.5 \times 10^{-3}\,\mathrm{cm^{-3}} > n_0 > 5 \times 10^{-4}\,\mathrm{cm^{-3}}$ and $1.6 \times 10^6\,\mathrm{K} > T_0 > 7 \times 10^5\,\mathrm{K}$, respectively, and where the density at the base of the corona is proportional to the atomic and molecular hydrogen density in the disk, $n_0 \propto n_{\mathrm{H\,I+H_2}}$. In addition, $T_0 = 1 \times 10^6$ K, $n_0 = 1 \times 10^{-3}\,\mathrm{cm^{-3}}$ in the favored model; the coronal mass is $7 \times 10^7\,M_\odot$, and the mass flux of clouds onto the disk is $2.4\,M_\odot\,\mathrm{yr^{-1}}$. With the assumption that clouds form individually, a model distribution of the velocities of clouds on the sky is given. Clouds spiral down onto the plane 3–60 $\times 10^7$ yr after formation and often intercept the plane slightly beyond where the gas originally entered the corona. This creates a circulation current in the disk which makes the metallicity gradient shallower than in a "closed" model of the Galaxy. Density perturbations which trigger cloud formation are probably coherent over a length of ~ 1 kpc. Because the corona rotates differentially, large perturbations, and later, cloud groups, are stretched in θ; this explains the occasional chainlike appearance of groups of high-velocity clouds.

Subject headings: galaxies: internal motions — galaxies: structure — insterstellar: matter — nebulae: general

I. INTRODUCTION

The high-velocity clouds of neutral hydrogen are common objects in the Galaxy, yet their origin remains unknown. Since these clouds reflect global activity within the Galaxy, by understanding them one can gain further insight into the physical processes active within our Galaxy as well as in other galaxies. Therefore, we are motivated to develop a successful explanation for the origin of these high-velocity clouds.

A cloud of neutral hydrogen above $b = 10°$ with a velocity greater than $80\,\mathrm{km\,s^{-1}}$ is termed a high-velocity cloud (HVC; see review by Hulsbosch 1975 and § II*a*). HVC are detected in every longitude and latitude region, and most clouds have negative velocities. Occasionally, HVC form prominent chains on the sky. Unfortunately, the distances to the clouds are poorly known, but the most widely accepted view is that they are a few kiloparsecs above the plane of the Galaxy (Silk 1974; Hulsbosch 1975; Oort 1978).

Explanations for the origin and position of the HVC

account for some of the clouds (e.g., clouds overhead), but fail to resolve other major features (e.g., clouds toward the anticenter; see discussion in § II*a*). The key to a successful model for the HVC is provided by an observational and theoretical result. First, the mass flux of clouds onto the plane is so large (1 $M_\odot$ or greater; Shapiro and Field 1976; Hulsbosch 1975) that accumulated infalling gas would overwhelm the disk gas in much less than a Hubble time unless the source of HVC is the disk gas. Second, it is theoretically well established that clouds can condense within a hot, gaseous galactic corona that is bound to the Galaxy (if a corona exists; Spitzer 1956; Field 1975*a*, *b*; Shapiro and Field 1976; Chevalier and Oegerle 1979). One may envision a cycle where some disk gas is converted to coronal gas that rises above the disk, only to condense into cold clouds that return to the disk (first suggested by Shapiro and Field 1976, and termed "galactic fountain").

The observational and theoretical basis for the existence of a corona has substantially increased since Spitzer's pioneering work. In the disk, soft X-rays are probably produced by tenuous gas ($n \sim 3 \times 10^{-3}$ cm^{-3}) with temperatures in the million degree range (e.g., Williamson *et al.* 1974; Sanders *et al.* 1977). The filling fraction for this hot interstellar medium ($f_{\rm HIM}$) is probably between 0.2 (Jenkins 1978) and 0.8 (McKee and Ostriker 1977); its presence is attributed to the occurrence of supernovae in the disk. This gas has an isothermal scale height of several kiloparsecs (Spitzer 1956), vastly greater than the thickness of the H I disk. If the filling factor is small, hot gas bubbles through the H I layer, but if $f_{\rm HIM} \approx 1$, hot gas flows freely into the halo. In either case, hot gas eventually escapes the galactic plane and, depending upon its temperature, either flows outward as a wind or attempts to reach equilibrium with the galactic gravitational potential (Field 1975*a*, *b*; McKee and Ostriker 1977; Chevalier and Oegerle 1979). If the cooling time is much longer than the time for gas to reach hydrostatic equilibrium, the scale height of the gas is independent of density. Eventually, radiative cooling causes coronal gas to undergo thermal instabilities (Field 1965), condense into neutral hydrogen clouds, and fall toward the plane (if its cooling time is less than a Hubble time; Spitzer 1956). Shapiro and Field (1976) point out that cooling may be rapid enough so that coronal gas condenses before reaching hydrostatic equilibrium. They suggest that these clouds fall toward the plane with velocities appropriate for the HVC, but they do not indicate if the major velocity features of the HVC can be reproduced (taken literally, their suggestion only explains the HVC observed overhead, not at lower latitudes).

Here, we investigate the galactic fountain and galactic corona models in detail to see whether the high- and intermediate-velocity clouds are actually produced this way. In §§ II*b* and II*c* we develop a model for the trajectories of clouds which matches all observational velocity features of the HVC; the positions for the formation of clouds is deduced (§ II*c*). Then we investigate the dynamics of a hot corona of cosmic abundance (§§ III, IV) and the condensation of clouds within it, and eventually, we combine the hydrodynamics of coronal gas with the appearance of HVC on the sky (§§ IV, VI).

II. KINEMATIC MODEL OF THE HIGH-VELOCITY CLOUDS

a) Observations

Neutral hydrogen clouds with velocities relative to the Sun of greater than 80 km s^{-1} are defined as high-velocity clouds (HVC). Intermediate-velocity clouds (IVC) refer to H I with line-of-sight velocities between 35 km s^{-1} and 80 km s^{-1}. Both the IVC and HVC are found in all longitude sectors and most of the HVC have latitude greater than 10°. Early maps of the HVC indicated that they all possessed negative velocities (Habing 1966; Muller *et al.* 1966; Hulsbosch and Raimond 1966; Hulsbosch 1968), and based upon this finding, Oort (1966, 1967, 1969, 1970) suggested that they were gas clouds being accelerated into the Galaxy by infalling intergalactic matter. Subsequent studies (Rickard 1971; Davies 1972*a*, *b*; Wannier, Wrixon, and Wilson 1972; and others) revealed the presence of positive velocities in the third and fourth quadrants, which led Davies (1972*a*, *b*) and Verschuur (1973; see 1975 review) to suggest that galactic rotation in a highly warped disk provided the velocities and high latitude of these clouds. While this is a convincing explanation for some HVC at low latitude, HVC toward the anticenter or at high galactic latitude remain unexplained (Hulsbosch and Oort 1973; Hulsbosch 1975; these two authors express some concern that the HVC at $l \approx 270°$ must be at least 30 kpc distant if galactic rotation causes them; in part, they refute the galactic rotation hypothesis). In the most recent maps of high-velocity H I, several investigators (see Davies 1975; Verschuur 1975; Hulsbosch 1975; Giovanelli 1978) find both high positive and negative velocity gas toward the anticenter (-200 km s$^{-1} \lesssim v_{\rm LOS} \lesssim +125$ km s^{-1}), high positive velocities near $l = 270°$ (240 km s$^{-1} \gtrsim v_{\rm LOS}$), and large negative velocities at high latitude ($b > 60°$, $|v_{\rm LOS}| \approx 130$ km s^{-1}, 130 km s^{-1} may be a poorly defined upper limit because the sample of clouds above 60° is small). In general, negative velocities are more frequent and of greater magnitude than positive velocities. The distances to these clouds are poorly known; the evidence indicates that at least some of the clouds are above the plane by several kiloparsecs (see discussion by Oort 1970; Silk 1974; Hulbosch 1975; Oort 1978; Oort and Hulsbosch 1978). Until further data become available, we assume that most IVC and HVC are above the plane. Because no current theory explains all gross properties of the HVC in a physically self-consistent model (Davies 1975; Hulsbosch 1975), we seek a new explanation and begin by developing a simple kinematic model. The most important and unambiguous observational details we hope to reproduce are (1) negative HVC at high latitude; (2) primarily negative HVC at $l \approx 90°$, $b < 30°$, and primarily high positive velocity clouds at $l \approx 270°$, $b < 30°$; (3) HVC

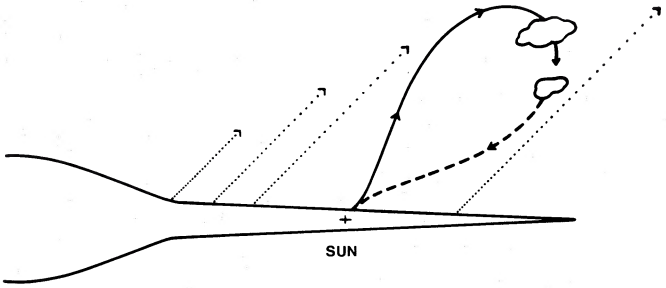

FIG. 1.—Hot gas rising from disk is denoted by dotted lines with an arrow. The solid and dashed lines illustrate the cycle in which gas moves upward and radially outward before suffering a thermal instability and forming into a cloud which falls toward its point of origin.

toward the anticenter at all latitudes; and (4) predominance of negative-velocity clouds. Also, HVC/IVC frequently appear in strings, and this feature is addressed in § VI*a*.

b) General Kinematic Models

We propose that hot gas forming the galactic fountain moves upward and radially outward before condensing into clouds (by thermal instabilities; Field 1965) that return ballistically toward the disk (see Fig. 1). The observed velocity of these clouds is a substantial sum of its velocity components in z, $\tilde{\omega}$, and θ. Since the clouds move ballistically, their trajectories and observed velocities can be simply calculated. Here we develop general models for their observed velocities and then apply them to the HVC (§ II*c*).

i) *Differential Rotation Velocity*

The line-of-sight velocity component arising from differential rotation is

$$u_\theta = (\dot{\theta}_0 - \dot{\theta}\tilde{\omega}_0/\tilde{\omega}) \sin(l) \cos(b)\,, \qquad (2.1)$$

where $\dot{\theta}_0$ and $\tilde{\omega}_0$ are the orbital velocity (km s^{-1}) and galactic distance of the Sun; $\dot{\theta}$ and $\tilde{\omega}$ are the velocity and position of the H I cloud. If $150° < l < 120°$, $u_\theta < 100$ km s^{-1}, and for $l = 180° \pm 10°$, u_θ is inconsequential regardless of what $\tilde{\omega}$ or $\dot{\theta}$ is (for $\dot{\theta} \lesssim \dot{\theta}_0$). However, for $\sin(l) \cos(b) > 0.5$, u_θ can be larger than 200 km s^{-1}.

In general, coronal gas above $\tilde{\omega}$ may have originated elsewhere in the disk ($\tilde{\omega}_i \neq \tilde{\omega}$), and, owing to pressure forces, may have been transported to $\tilde{\omega}$ (model *a*). If coronal gas retains its angular momentum as it moves from $\tilde{\omega}_i$ to $\tilde{\omega}$, its rotational velocity changes, so the corona and disk do not corotate. Alternatively, coronal gas may rise upward but remain at $\tilde{\omega}_i$ and more nearly corotate with the disk (model *b*). To investigate these models, we use a flat rotation curve for the Galaxy. The differential rotational velocity which arises in model *b* is plotted in Figure 2. Even at low latitudes and $l \approx 90°$, 270°, where $\sin l \cos b = 1$, u_θ remains small until $\tilde{\omega} > 20$ kpc; $u_\theta = 150$ km s^{-1} for $\tilde{\omega} = 25$ kpc and $u_\theta = 200$ km s^{-1} for $\tilde{\omega} = 50$–70 kpc (depending on values chosen for $\tilde{\omega}_0$ and $\dot{\theta}_0$). Gas near

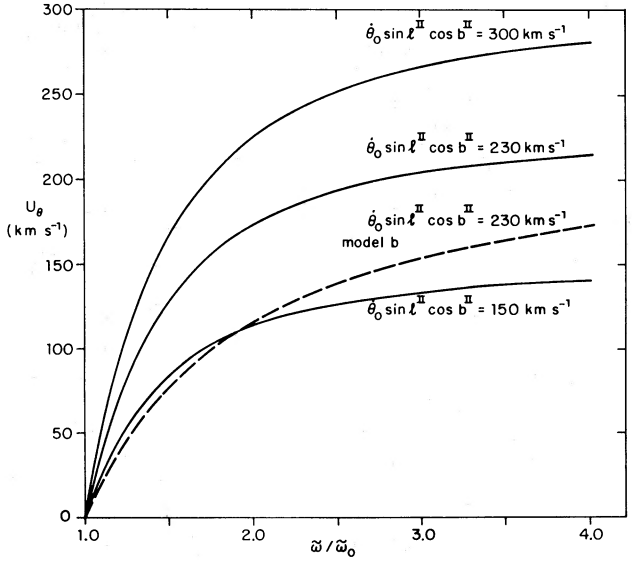

FIG. 2.—Observed differential velocity is plotted against position of a cloud with respect to solar circle ($\tilde{\omega}/\tilde{\omega}_0$). The dashed line results from gas in stable rotation in the galactic disk (model *b*) and the solid lines are for clouds represented by model *a*. The number above each line is the rotational velocity at the solar circle times a geometrical reduction factor.

the solar circle ($\tilde{\omega} \approx \tilde{\omega}_0$) has no circular velocity regardless of latitude or longitude.

If there is reason to expect gas to move radially, model *a* is more appropriate than model *b*. The thermal energy of coronal gas is comparable to, but less than, the potential field of the Galaxy. Similarly, pressure gradients in the hot gas are comparable to Galactic gravitational forces. Therefore, because the pressure of hot gas rising from the disk may be a function of radius, a pressure gradient exists at the base of the corona which forces gas to flow radially before attaining a new equilibrium position at $\tilde{\omega}$. As the gas moves, suppose that it conserves its angular momentum (initial angular momentum is $j_i = \tilde{\omega}_i \dot{\theta}_i$). When a cloud condenses, it will have a rotational line-of-sight velocity given by

$$u_\theta = (\dot{\theta}_0 - \dot{\theta}_i \tilde{\omega}_i \tilde{\omega}_0 \tilde{\omega}^{-2}) \sin(l) \cos(b) . \quad (2.2)$$

As an example, observe gas rising from the solar neighborhood; $\dot{\theta}_i \tilde{\omega}_i = \dot{\theta}_0 \tilde{\omega}_0$ and u_θ is given in Figure 2. For the same position of cloud formation $\tilde{\omega}$, much larger values of u_θ are possible in this model *a* than in model *b*. As seen in the example given in Figure 2, $u_\theta = 150$ km s^{-1} for $\tilde{\omega} = 15$ kpc (instead of 25 kpc). If gas that forms into clouds at $\tilde{\omega}$ originated interior to the solar circle ($\tilde{\omega}_i < \tilde{\omega}_0$, but $\tilde{\omega} > \tilde{\omega}_0$), u_θ reaches these velocities at lower $\tilde{\omega}$ than in the above example; with $\tilde{\omega}_i = 6$ kpc, $u_\theta = 150$ km s^{-1} for $\tilde{\omega} = 12$ kpc. Another aspect of model *a* is that clouds now at the solar circle may have a significant u_θ ($\lesssim 100$ km s^{-1}) solely because gas comprising the cloud did not originate at $\tilde{\omega}_0$.

The amplification of simple galactic rotation (model *a* compared to model *b*) arises because $j = \tilde{\omega}\dot{\theta}$ is constant while a mass element is moved outward ($\tilde{\omega}$ increases), hence $\dot{\theta}$ decreases. Therefore, the rotational velocity difference between the Sun and a radially displaced cloud at $\tilde{\omega}$ is much greater than the rotational velocity difference between the Sun and the disk at $\tilde{\omega}$. If the Galaxy were characterized by a Keplerian rotation curve exterior to the solar circle, then simple differential galactic rotation is more effective at producing large u_θ in model *b*; model *a* is unaffected. However, no convincing evidence for a Keplerian rotation curve exists, and some studies indicate the rotation curve is nearly flat (Jackson, Fitzgerald, and Moffat 1978; Blitz 1979), consistent with Rubin's (1978) finding for external galaxies.

ii) *Radial Velocity*

In order for a cloud to attain nonzero radial velocity, the element of gas from which it forms must feel different forces before and after formation. This occurs naturally if the corona is in static equilibrium in the radial direction because pressure forces and centrifugal forces balance gravity. As a condensation cools, its radial pressure support vanishes and it begins to fall toward its original radial position at velocity $u_{\tilde{\omega}}$ (this is model *a*; no radial velocities are produced in model *b*). Consider an element of gas with angular momentum $j = \dot{\theta}_i \tilde{\omega}_i$ (*i* denotes its original position and velocity in the disk) which forms a cloud at $\omega_f (\tilde{\omega}_f > \tilde{\omega}_i$; this is a model *a* described above). Acceleration of the cloud is given by

$$\frac{du_{\tilde{\omega}}}{dt} = -\frac{\partial \Phi}{\partial \tilde{\omega}} + \frac{j_i^2}{\tilde{\omega}^3} , \quad (2.3)$$

where $\partial\Phi/\partial\tilde{\omega}$ is the radial galactic gravitational force. If the rotation curve is flat in the region of interest ($\partial\Phi/\partial\tilde{\omega} = \dot{\theta}_i^2/\tilde{\omega}$), the solution to equation (2.3) is

$$u_{\tilde{\omega}} (\dot{\theta}_i \cos b \sin\psi)^{-1} = \left\{ -\left(\frac{\tilde{\omega}_i}{\tilde{\omega}_f}\right)^2 \left[\left(\frac{\tilde{\omega}_f}{\tilde{\omega}}\right)^2 - 1 \right] + \ln \left(\frac{\omega_f^2}{\tilde{\omega}^2}\right) \right\}^{1/2} , \quad (2.4a)$$

where

$$\sin\psi = \left(1 - \frac{\tilde{\omega}_0^2}{\tilde{\omega}^2} \sin^2 l\right)^{1/2} \text{ for } |l| > \sin^{-1}\left[\min\left(\frac{\tilde{\omega}}{\tilde{\omega}_0}, 1\right)\right], \quad -\pi \le l \le \pi ,$$

$$= -\left(1 - \frac{\tilde{\omega}_0^2}{\tilde{\omega}^2} \sin^2 l\right)^{1/2} \text{ for } |l| < \sin^{-1}\left[\min\left(\frac{\tilde{\omega}}{\tilde{\omega}_0}, 1\right)\right], \quad -\pi \le l \le \pi . \quad (2.4b)$$

In Figure 3, $u_{\tilde{\omega}} (\dot{\theta}_i \cos(b) \sin\psi)^{-1}$ is calculated as a function of $\tilde{\omega}/\tilde{\omega}_i$ for different values of $\tilde{\omega}_f/\tilde{\omega}_i$. Each line is a cloud trajectory which begins at zero velocity

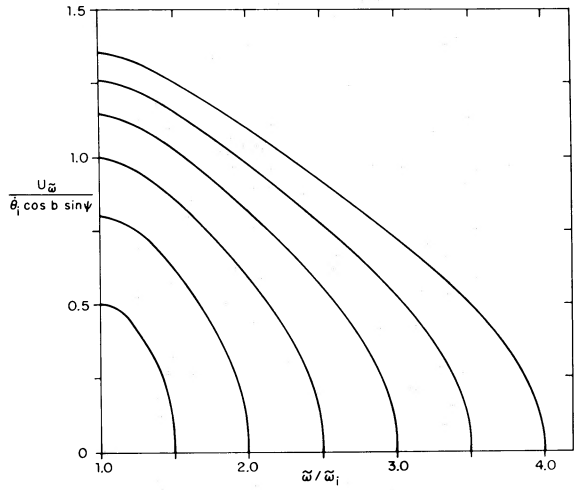

FIG. 3.—Radial velocity of an infalling cloud ($u_{\tilde{\omega}}$) is divided by a geometrical factor and the rotational velocity the cloud gas initially had at its point of origin in the disk ($\tilde{\omega}_i$). The abscissa is the cloud position in units of $\tilde{\omega}_i$. Each line represents a cloud trajectory for clouds which form with zero radial velocity ($u_{\tilde{\omega}} = 0$ is the beginning of each trajectory). Clouds reach their maximum velocity at $\tilde{\omega} = \tilde{\omega}_i$, which is where their acceleration changes sign.

and proceeds inward until it intercepts the disk near $\tilde{\omega}/\tilde{\omega} = 1$. The maximum streaming velocity occurs as the cloud passes over its original position $\tilde{\omega} = \tilde{\omega}_i$. At the point of formation, if the streaming velocity of clouds is small with respect to $\dot{\theta}_i$, and if gas moved outward ($\tilde{\omega}_f > \tilde{\omega}_i$), $u_{\tilde{\omega}}$ is always negative in the direction away from the galactic center [$\cos(b) \sin\psi > 0$]. Positive velocities are also produced as clouds move interior to the solar circle ($\tilde{\omega} < \tilde{\omega}_0$), and the effect is greatest near the galactic center.

iii) *Vertical Velocity*

At high galactic latitude, the line-of-sight velocity arising from u_θ and $u_{\tilde{\omega}}$ is small because $\cos(b) \to 0$ as $b \to 90°$; only u_z contributes to the total line-of-sight velocity $v_{\rm LOS}$. Coronal gas is maintained vertically entirely through pressure support. Clouds condensing from the corona no longer feel any force from the pressure gradient in the hot gas, and they fall ballistically under the influence of gravity. A cloud's observed velocity is

$$u_z = \left(\dot{Z}_f - \int_{z_f}^{z} \frac{\partial\Phi}{\partial z}\, dz\right) \sin b\,, \qquad (2.5)$$

where $\dot{Z}_f$ is its velocity at formation; Z_f is its position at formation; $\partial\Phi/\partial z$ is the gravitational force; and Z is the height at which the cloud is observed. A cloud spends the least amount of time at high velocities and the greatest amount of time at low velocities. We use the Innanen (1973) model for $\partial\Phi/\partial\tilde{\omega}$ in order to estimate u_z for $\dot{Z}_f = 0$, $\sin b = 1$. For a cloud which has zero velocity at z, Table 1 indicates the maximum value for u_z, which occurs as the cloud reaches the plane.

Clearly, in the region away from the galactic center ($270° \gtrsim l \gtrsim 90°$) the observed velocity of a cloud formed in the corona cannot be greater than the escape velocity from the Galaxy at the solar circle. The local escape velocity is conventionally estimated to be 360 km s^{-1}, but it may be closer to 560 km s^{-1} if the Galaxy possesses a massive halo (Ostriker 1978).

c) Fitting the Model to the High-Velocity Clouds

All major features in the velocity distribution of IVC and HVC can be explained if the galactic fountain flows upward and outward from the disk (model *a* is valid). At high latitude only $\hat{Z}$ velocities are seen, while toward the anticenter and at low latitude ($b < 30°$), only streaming motion contributes to the line-of-sight velocity. The third velocity component, u_θ, cannot similarly be isolated because it requires that the position of the cloud is known, which it is not.

TABLE 1

FREE-FALL VELOCITY U_z (km s^{-1})

Z (kpc)	$\tilde{\omega}$ (kpc)			
	7	9	13.5	18
1.....	45	35	19	10
2.....	100	77	35	18
5.....	184	148	77	45
10.....	253	210	126	77
20.....	310	268	179	126

Near the anticenter ($l \approx 180°$, $|b| < 20°$), negative velocities up to -200 km s^{-1} are known (Hulsbosch 1978; Oort 1979). In our model, this radial streaming is explained if the position where the most rapidly moving clouds form is at least twice its initial position ($2 \lesssim \tilde{\omega}_f/\tilde{\omega}_i \lesssim 3$ for $\sin l \cos b = 1$). Slower clouds either formed closer to their initial position, or have not yet reached maximum velocity. Radial return of gas could easily produce the negative velocity clouds found at low galactic latitude near the anticenter (HVC and IVC). A consequence of this model is that positive velocity clouds exist toward the galactic center at $b < 20°$. While this region is often excluded from surveys, some positive IVC are observed there (see map in Verschuur 1975).

Directly overhead one detects only the vertical velocity of clouds (u_z, $b > 60°$). The highest velocities ($|u_z| > 80$ km s^{-1}) are all negative and up to -150 km s^{-1}. If large positive velocities existed, we would conclude that clouds formed in the upward flow ($t_{\rm cool} < t_{\rm eq}$). This is, however, not the case, so $t_{\rm cool} \gtrsim t_{\rm eq}$ (small positive or negative velocity at formation)—*the corona is nearly hydrostatic in the vertical direction.* Clouds falling from 5 kpc $< z <$ 10 kpc easily attain the highest observed velocities (Table 1), while slower clouds either formed at lower elevation, or have not yet significantly fallen after forming.

There are two positions in the sky where u_z is unimportant and $u_{\tilde{\omega}}$ may be small (if clouds are nearby, 8 kpc $< \tilde{\omega} <$ 12 kpc): at $b < 30°$ and $l \approx 90°$ or 270°. Because velocities are positive at $l \approx 270°$ and negative at $l \approx 90°$, we propose that these high velocities ensue from amplified differential rotation of clouds with respect to the Sun (model *a*). Earlier, Davies (1972*a*, *b*) and Verschuur (1973, 1975, and references therein) first noticed that in a crude sense, the velocity of the IVC and HVC changes sign between the second and third longitude quadrants, so they suggested that u_θ must be an important component of these clouds. They chose model *b* which predicts velocities lower than model *a*, which we favor. Because clouds naturally form high above the plane in our model, we obviate the need for an extremely warped galactic plane (e.g., Verschuur 1975), a severely criticized suggestion (Hulsbosch and Oort 1973; Hulsbosch 1975).

The negative velocities at $l \approx 90$ are easily explained if gas moved outward about twice its original position ($v_{\rm LOS} = -149$ km s^{-1}; $\tilde{\omega}_f \approx 2\tilde{\omega}_i$, $\tilde{\omega}_i \approx$ 6–8 kpc). At $l \approx 270$, most positive velocities ($v_{\rm LOS} < +200$ km s^{-1}) are explained by gas moving 2–3 times its original position ($\tilde{\omega}_f/\tilde{\omega}_i =$ 2–3, $\tilde{\omega}_i \approx$ 6–8 kpc). However, $v_{\rm LOS}$ is as large as $+240$ km s^{-1} in a few clouds (Giovanelli and Haynes 1976), so either $\dot{\theta}_0 > 240$ km s^{-1}, radial streaming contributes to $v_{\rm LOS}$ (§ IV*b* [ii]), or these clouds are not associated with the corona. Note that

the maximum $u_{\tilde{\omega}}$ and u_z velocities occur as clouds near their point of origin.

Throughout the rest of the sky, negative velocity clouds are more frequent and of larger velocity than their positive velocity counterparts. This occurs because $v_{\rm LOS}$ is the sum of $u_{\tilde{\omega}}$, u_θ, and u_z; however, positive velocities are primarily contributed only from the u_θ component.

The details of the fountain change if the true galactic mass model differs from the adopted one. If $\dot{\theta}_0 >$ 230 km s^{-1}, the radial travel of the fountain ($\tilde{\omega}_f/\tilde{\omega}_i$) is decreased, and if the galactic potential well is deeper than we assumed (i.e., massive disk external to the Sun), u_z was underestimated (in both cases high velocities are easier to achieve). The hydrodynamics of the fountain may be overly simplified—n_0 and T_0 may be functions of θ (spiral arms) and there may be local enhancements in n and T which could lead to turbulence in the corona. Also, circulation currents may exist in the corona (Waxman 1978). These effects may help explain those HVC with unusual characteristics.

Despite random features in the velocity field, by fitting a kinematic model to the gross velocity features of the IVC and HVC, strong constraints are placed on the position of cloud formation. In conclusion, the primary features of the galactic fountain are as follows: (1) it flows upward to $Z \approx$ 5–10 kpc before clouds condense: (2) $t_{\rm cool} \gtrsim t_{\rm eq}$ in Z; (3) gas flows radially to $\tilde{\omega}_f/\tilde{\omega}_i \approx$ 2–3 before condensing; (4) some clouds probably form in the radial flow, or $t_{\rm cool} \lesssim t_{\rm eq}$ in $\tilde{\omega}$; (5) elements of gas retain their angular momentum as they flow upward and outward.

Although the picture outlined above roughly accounts for the observations, it does not reveal how the clouds formed in the desired positions. In the following sections we develop a hydrodynamic representation for the corona and match it to the kinematic model of the clouds to produce a unified and self-consistent description of the HVC.

III. THE CORONA IS NOT STATIC

Here we investigate the possible existence of a static corona, the simplest useful physical model. To do this, we consider only the corona in the vertical direction and assume that coronal gas is enriched, which it must be if it was originally part of the interstellar medium.

A static corona must satisfy the time-independent momentum equation (pressure support balances gravity) and heating must balance cooling throughout the corona for at least a Hubble time. The corona is subject to boundary conditions—its pressure cannot fall below that of the intergalactic medium ($P_{\rm IGM}$). Field and Perrenod (1977) predict $P_{\rm IGM}/k < 10^3$ K cm^{-3}, but the actual value of $P_{\rm IGM}/k$ is not critical to this discussion as long as $P_{\rm IGM}/k > 0$. A final point is that the static corona must be dynamically and thermally stable.

When condition can be neglected, the corona is not isothermal, and the temperature must decrease upward. At every point in the corona, heating due to supernovae and the X-ray background (proportional to n) must balance radiative cooling (proportional to n^2). The solution for a static corona can be easily found, and the corona is dynamically stable against convection. However, the corona is thermally unstable (Field 1965), and instabilities grow during a cooling time scale, which is shorter than a Hubble time for $n > 6 \times 10^{-6}$ cm^{-3} (after Shapiro and Moore 1976). Without conduction, the corona is not static.

If conduction is very important, the entire corona is isothermal, and all small-scale thermal instabilities are suppressed. Once again, a dynamically stable solution can be found, and while small-scale thermal instabilities do not grow in the corona, the entire structure of the corona is thermally unstable. With a few differences, the instability analysis is similar to that by Field (1965) and will not be repeated here. For a slight compression of the corona, the density increases and cooling begins to overwhelm heating as in the standard thermal instability scenario. A slight expansion of the corona (density decreases) causes heating to dominate cooling, and the corona eventually escapes as a wind. These perturbations can arise from passing companion galaxies, changes in the heating rate, or a change in $P_{\rm IGM}$. So regardless of the role of conduction, the corona cannot remain static if its temperature lies in a thermally unstable regime (2×10^5 K $< T < 10^7$ K). Furthermore, we calculate that dust is also unable to suppress the thermal instability.

We conclude that *hot gas must rise above the disk, and if the gas remains bound to the Galaxy, it will form a corona that is not static.* Because of a thermal instability between 2×10^5 K and 10^7 K, regions in the corona must cool; these regions are small if conduction is unimportant but comparable to the size of the corona if conduction is efficient.

IV. HYDRODYNAMIC MODELS FOR THE CORONA

a) Boundary Conditions and Parameters

i) *Influx of Hot Gas into the Corona*

To properly construct hydrodynamic models for the corona, one must have an accurate model for the interstellar medium; the supernova frequency and heating rate as a function of Z, the filling factor for the hot interstellar medium ($f_{\rm HIM}$), and the values of $n_{\rm HIM}$, $T_{\rm HIM}$ as a function of Z. Unfortunately, the density and temperature at the base of the corona depends sensitively upon poorly known quantities, such as the scale heights of supernovae and disk gas. One does know that the gas cannot be hot enough to cause a wind, as clouds cannot form in a wind (Chevalier and Oegerle 1979).

Rather than a wind, we favor a corona which is supplied with gas by hot clouds percolating through the H I layer. Supernovae that break through the plane into the corona (Chevalier and Gardner 1974), and supernovae that occur in the corona supply heat

to the coronal gas. If most of this heating occurs primarily near the base of the corona (Z_c), it is fair to fix n, T at Z_c. We will consider heating and cooling in a column of corona gas above the disk. The cooling rate in the column is given by

$$L = \int_0^\infty n_e^2 \Lambda dZ\,, \tag{4.1}$$

where the cooling function for a gas of cosmic abundance is $\Lambda = 6.2 \times 10^{-19} T^{-0.6}$ ergs cm^3 s^{-1} (10^5 K $< T < 2 \times 10^7$ K, from McKee and Cowie 1977). So for an adiabatic density distribution in Z and $(T/T_0) = (n/n_0)^{2/3}$, equation (4.1) can be written as

$$L = 2 \times 10^{-6} \left(\frac{n_0}{1 \times 10^{-3}}\right)^2 \left(\frac{T_0}{1 \times 10^6 \text{ K}}\right)^{0.4} \times (g_z/10^{-8} \text{ cm s}^{-2})^{-1} \text{ ergs cm}^{-2} \text{ s}^{-1}\,, \tag{4.2}$$

where n_0 and T_0 are defined at the base of the corona. The stars in the spherical or bulge component of the Galaxy probably have a supernova rate like E/S0's. From Tammann's (1977) work, this is 0.18–0.19 SN 10^{-2} yr^{-1} $10^{-10} L_\odot^{-1}$. Recently, de Vaucouleurs (1978) estimated $L = 1.64 \times 10^{10} M_\odot$ for the Galaxy; 0.34 L is attributed to the bulge. We use our mass model for the Galaxy (§ IVa[ii]) to estimate the column density of bulge stars above the solar circle and thereby estimate the integrated supernova heating rate

$$H_b = 2 \times 10^{-7} \left(\frac{E}{10^{51} \text{ ergs}}\right) \text{ ergs cm}^{-2} \text{ s}^{-1}\,, \tag{4.3}$$

where E is the supernova energy. Clearly, supernova heating by the bulge near the sun is small compared to radiative cooling.

The main heat source for the corona must arise from supernovae which break through the hydrogen layer. Locally, the supernova rate is $\sim 10^{-13}$ SN pc^{-3} yr^{-1} and the supernova scale height is ~ 55 pc. The total energy released by supernova between $Z' = \infty$ and $Z' = Z$ is

$$H_d(Z) = 2 \times 10^{-5} \left(\frac{E}{10^{51} \text{ ergs}}\right) \times \exp(-Z/55 \text{ pc}) \text{ ergs cm}^{-2} \text{ s}^{-1}\,. \tag{4.4}$$

Chevalier and Gardner (1974) point out that supernova of $\sim 10^{51}$ ergs will break out of the H I layer only if they occur more than one scale height above the plane ($Z > 100$ pc). Unfortunately, the supernova rate and $Z/55$ pc are not known well enough to accurately calculate H_d, but for $Z \gtrsim 100$ pc, we see that $H_d L^{-1} \lesssim 1$ (i.e., heating is about the same as, or less than, cooling). Locally, the primary heat source for the corona comes from the disk, not the bulge. Also, heating by the X-ray background is known to be small (Weisheit and Collins 1976).

In conclusion, we feel that a corona rather than a wind emanates from the disk, and that the corona can be characterized by choosing n and T at the base of the corona. This approach is similar to that used by Chevalier and Oegerle (1979) and has the advantage that a large number of poorly known variables are replaced by just two, which in principle can be observationally determined.

ii) *Mass Model for the Galaxy*

Rotation curves of external disk galaxies are flat even past their optical images (Rubin 1978; Krumm and Salpeter 1976), and recent evidence indicates that the Galaxy also has an approximately flat rotation curve beyond the Sun (Jackson, Fitzgerald, and Moffat 1978; Blitz 1979). Therefore, due to the commonness of flat rotation curves, we construct a mass model for the Galaxy by using Innanen's (1973) "representative model" in addition to an extended halo of the form

$$\mathcal{M}_{\text{halo}} = M_h x^3 (1 + x)^{-2}\,, \tag{4.5a}$$

$$x = (\tilde{\omega}^2 + Z^2)^{1/2} r_b^{-1}\,, \tag{4.5b}$$

where $r_b = 13$ kpc, and $M_h = 1.35 \times 10^{11} M_\odot$. The halo is terminated at 100 kpc, out to which the rotation curve is roughly flat, asymptotically approaching 220 km s^{-1} exterior to the solar circle. The rotation velocity at the solar circle ($\tilde{\omega}_0 = 9$ kpc) is $\theta_0 = 230$ km s^{-1} (Oort and Plaut 1974). The escape velocity from the solar circle of 541 km s^{-1} is very sensitive to the tidal cutoff of the extended halo, so the close agreement with Ostriker's (1978) value of 558 km s^{-1} is fortuitous.

Within 20 kpc of the galactic center, the extended halo has little influence on the gravitational field of the Galaxy because the Innanen model dominates the mass distribution there. To illustrate this, the potential drop between $\tilde{\omega} = 9$ kpc, $Z = 0$ and $\tilde{\omega} = 15$ kpc, $Z = 0$ is 3×10^{14} cm^2 s^{-2}, only one-sixth of which arises from the presence of the extended halo. Because the regions of most prolific cloud formation primarily feel the gravitational force of Innanen's model, the extended halo does not strongly affect our results (for $T > 2 \times 10^6$ K, the extended halo plays a very important role).

b) Hydrodynamic Modeling

There are several constraints on the local value of n and T. First, the pressure must be less than that in the disk (1); otherwise, back pressure from the halo would compress the ISM to bring it into pressure equilibrium. X-ray measurements in the 0.5–2 keV range must not be exceeded by the coronal gas (2). We also demand that (3) n be high enough so that radiative cooling exceeds supernova heating, that (4) the velocity distribution of the HVC reproduce the observations, and that (5) T be low enough so that a wind cannot occur in the local neighborhood.

A major obstacle to the above model is that n and T, which are not even well known near the Sun, must be specified as a function of $\tilde{\omega}$ and θ. We avoid this dilemma by examining a few general forms of n and T which represent the most probable physical conditions.

TABLE 2

HYDRODYNAMIC MODELS FOR THE CORONA

Model	n_0[a] (cm^{-3})	T_0[a] (K)
	n_0, T_0 independent of $\tilde{\omega}$	
A1	3×10^{-3}	5×10^5
A2	1×10^{-3}	5×10^5
A3	3×10^{-4}	5×10^5
B1	3×10^{-3}	1×10^6
B2	1×10^{-3}	1×10^6
B3	3×10^{-4}	1×10^6
C1	3×10^{-3}	2×10^6
C2	1×10^{-3}	2×10^6
C3	3×10^{-3}	2×10^6
	T_0 constant, $n_0 \propto n_{\mathrm{H\,I+H_2}}$	
D1	1×10^{-3}	5×10^5
D2	3×10^{-3}	5×10^5
E1	1×10^{-3}	1×10^6
E2	6×10^{-4}	1×10^6
E3	3×10^{-4}	1×10^6
F1	1×10^{-3}	2×10^6
F2	3×10^{-4}	2×10^6

[a] Density and temperature at the base of the corona directly above the solar neighborhood, $\tilde{\omega} = 8.7$ kpc.

The basic numerical model used in this analysis is a two-dimensional hydrodynamic code with symmetry in θ, which includes galactic rotation and radiative cooling (see full description in Bregman 1978). The time-dependent accuracy is 5–10% yr throughout one entire run, which covers about 1–6 $\times$ 10^8 yr and 1000 cycles. The grid size was 15–28 kpc in $\tilde{\omega}$ and between 4.5 and 21 kpc in Z, depending on T_0; a 40 $\times$ 32 grid was used, but 28 $\times$ 22 and 60 $\times$ 44 grids were used in some runs. Model parameters are listed in Table 2.

Clouds form when a zone radiatively cools below 10^4 K so that the recombination time is less than one time step (rarely are two or more zones involved). The density or pressure perturbation that grows into a cloud arises from numerical noise. Clouds are removed from the grid and replaced by the average pressure and density of the surrounding medium. This method does not obviously stimulate cloud formation elsewhere (e.g., no chain reactions).

i) *Height of Cloud Formation*

We now search for the functions $n(\tilde{\omega})$ and $T(\tilde{\omega})$ for which clouds form in the positions outlined above (§ IIc). To determine the height of cloud formation, we initially treat the problem only in $\hat{Z}$ and ignore gas motions in $\hat{\omega}$ and $\hat{\theta}$. As the hot gas escapes the plane, it rushes upward into the coronal gas at roughly the sound speed and attempts to establish itself in hydrostatic equilibrium. The time required to reach equilibrium is the adiabatic density scale height divded by some multiple of the sound speed, or

$$t_{\mathrm{eq}} = h/bc\,, \tag{4.6}$$

$$h = 6.5\left(\frac{T}{10^6\ \mathrm{K}}\right)\left(\frac{g}{10^{-8}\ \mathrm{cm\ s^{-2}}}\right)^{-1}\mathrm{kpc}\,, \tag{4.7}$$

where c is the adiabatic sound speed, b is a correction factor determined from numerical models, and g is the mean gravitational field above the plane ($g \approx 2\pi G\sigma$). It is necessary and correct to use the adiabatic assumption here ($\gamma = 5/3$); this is discussed later. As the gas rises, it cools after approximately

$$t_{\mathrm{cool}} = \frac{3kT}{2\Lambda n} = 4.2 \times 10^7\left(\frac{T}{10^6\ \mathrm{K}}\right)^{1.6} \times \left(\frac{n}{10^{-3}\ \mathrm{cm^{-3}}}\right)^{-1}\mathrm{yr}\,, \tag{4.8}$$

and if $t_{\mathrm{cool}} < t_{\mathrm{eq}}$, hydrostatic equilibrium never occurs. Nevertheless, through hydrodynamic simulations A, B, and C we find that the density scale height of the gas [where $n(Z)/n_0 = 1/e$] follows the law (to within 20%)

$$S = h[1 - \exp(-t_{\mathrm{cool}}/t_{\mathrm{eq}})]\,, \tag{4.9a}$$

or

$$S = 6.5\left(\frac{T}{10^6\ \mathrm{K}}\right)\left(\frac{g}{10^{-8}\ \mathrm{cm\ s^{-2}}}\right)^{-1} \times \left\{1 - \exp\left[-2.4\left(\frac{T}{10^6}\right)^{1.1}\left(\frac{n}{10^{-3}\ \mathrm{cm^{-3}}}\right)^{-1} \times \left(\frac{g}{10^{-8}\ \mathrm{cm\ s^{-2}}}\right)\right]\right\}\mathrm{kpc}\,. \tag{4.9b}$$

In the context of equations (4.6) and (4.9b), we find that the constant b is approximately 2.4. The physical basis for equation (4.9) is that when $t_{\mathrm{eq}} \ll t_{\mathrm{cool}}$ the gas reaches hydrostatic equilibrium, but if $t_{\mathrm{eq}} \gg t_{\mathrm{cool}}$, the scale height occurs where the gas cools, which is the product of the cooling time and the mean gas velocity (roughly the sound speed). Although the temperature resolution around clouds is lost when the gas forms clouds (at all grid sizes and zone spacings), the spatial distribution for cloud formation remains the same.

Not all clouds form at the same height; there is a spread in Z about S. The mass-weighted mean position for cloud formation in the coronal gas is at one density scale height S (to within 20%; numerical models A–C). Very few clouds form below 0.70 S but some low-mass clouds form up to 2S as seen in Figure 4. There is good reason to believe that clouds should form at the top of the corona and that these results are not artifacts of the numerical scheme. If rising gas moves at the sound speed, when $t_{\mathrm{cool}} \ll t_{\mathrm{eq}}$ we find that the gas cools more rapidly than it can decelerate due to loss of buoyancy so it forms at $Z \approx S$. In this regime, clouds form with positive upward velocity. For $t_{\mathrm{cool}} \gg t_{\mathrm{eq}}$, the cooling time in an adiabatic gas is $t_{\mathrm{cool}} \propto T^{1+f}n^{-1} \propto n^{[2(f+1)-3]/3}$, and since $0.6 < f < 1.0$ for $10^{5.3}$ K $< T < 10^7$ K (McKee and Cowie 1977; Cox 1972; Raymond, Cox, and Smith 1976) we see that

$$\frac{1}{15} < \frac{2f-1}{3} < \frac{1}{3}$$

so that t_{cool} *decreases for increasing* Z. The highest material therefore cools most rapidly, loses its

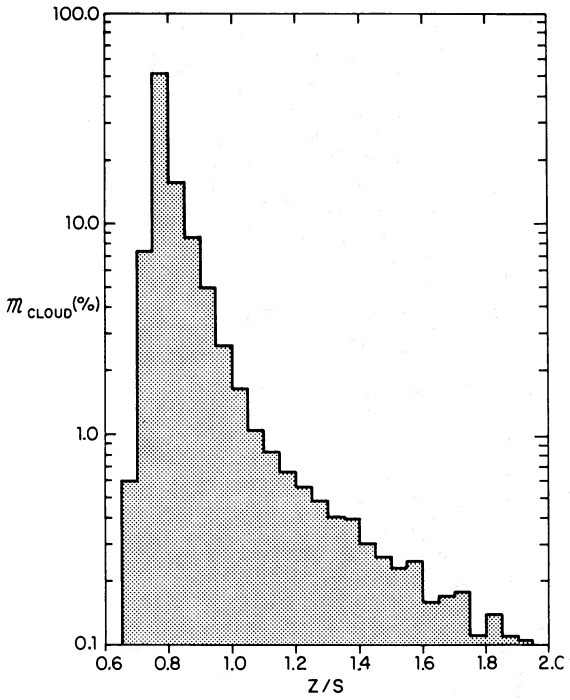

FIG. 4.—The percentage of clouds by mass is displayed in this histogram as a function of their dimensionless formation height (the cloud height divided by the density scale height of the corona). While the data for this histogram are drawn from models A–C, the functional dependence of $\mathcal{M}_{cloud}$ versus Z/S is also found in models D, E, and F.

buoyancy, and begins to fall into a higher-pressure region. Heating and cooling in the cloud are now controlled by radiative losses so as it is further compressed in higher pressure regions it radiates prodigiously and becomes a neutral cloud. Because of the low density at two scale heights only low-mass clouds can form (as numerical simulations confirm) while the constant upward mass flux and the longer cooling time prevents clouds from forming at the base of the corona. Clouds formed in this $t_{eq} \ll t_{cool}$ regime have negative velocities which must be less than the sound speed in the surrounding gas.

Values for the local temperature and density of the corona can now be obtained. The height of formation of the clouds, with the provision $t_{eq} < t_{cool}$ ($Z \approx$ 5–10 kpc, § II*c*) provides one functional constraint on T and n (eq. [4.9b] is used). Together with the condition $P_{corona} \leq P_{ISM}$ and that radiative cooling is greater than supernova heating, we calculate that at the base of the corona,

$$1.5 \times 10^{-3}\ \mathrm{cm}^{-3} > n_0 > 5 \times 10^{-4}\ \mathrm{cm}^{-3},$$
$$1.6 \times 10^{6}\ \mathrm{K} < T_0 < 7 \times 10^{5}\ \mathrm{K}.$$

ii) *The Radial Pressure Gradient*

For each choice of $n_0(\tilde{\omega})$, $T_0(\tilde{\omega})$, a radial pressure gradient is specified at the base of the corona. Even if hot gas has no pressure gradient at $Z \approx 0$, it must move outward as it rises above the disk. When the pressure gradient is zero at the base of the corona, no radial-pressure force exists, and since gravitational and centrifugal forces balance the gas feels no acceleration. However, as the gas rises upward to its natural scale height, the radial gravitational force diminishes while the centrifugal acceleration remains constant, giving rise to a net positive acceleration; gas moves outward until it reaches equilibrium.

In general, the pressure gradient at $Z \approx 0$ is nonzero, and if it is negative (P decreases outward), coronal gas experiences outward acceleration. The hot interstellar medium is probably related to the density of atomic and molecular gas in the disk, and since both decrease radially outward, one might expect a negative pressure gradient in the Galaxy. To summarize, there are two effects causing coronal gas to flow outward: the radial-pressure gradient and the decreasing radial gravitational force with height. Since the latter effect is governed by the mass model of the Galaxy, our only freedom is in the choice of the pressure gradient [given by $n_0(\tilde{\omega})$ and $T_0(\tilde{\omega})$], which must be chosen such that some coronal gas travels 2–3 times its original position (§ II*c*).

From the theory of the hot interstellar medium one cannot actually predict $n_0(\tilde{\omega})$ and $T_0(\tilde{\omega})$, so we assume that $n_0 \propto n_{H\,I+H_2}$ and T_0 is constant (a simple and possibly natural choice). Since $n_{H\,I+H_2}$ has a maximum at $\tilde{\omega} = 5.5$ kpc and rapidly decreases outside $\tilde{\omega} =$ 6 kpc (Gordon and Burton 1976), a very steep pressure gradient is created outside 6 kpc. From the numerical models D, E, and F we find that gas will not travel 2–3 times its radial position unless $T_0 > 5 \times 10^5$ K; in model E some gas traveled from 6 kpc to 13.5 kpc while in model F, some gas from 6 kpc traveled to 17 kpc. Of the models where $T_0 = 1 \times 10^6$ K (model E), the most successful ones were E1 and E2. Model E3 must be eliminated because radiative cooling is much less than supernova heating. In model E1, some clouds ($\sim 10\%$) form with significant outward radial velocity (> 100 km s^{-1}); this does not occur in model E2 because the cooling time is longer. We note that near the solar circle (model E1), the density and temperature are nearly constant in the vertical direction for about a scale height, even though most of the gas above us originated interior to the solar circle. The mass of the hot corona in model E1 is $7 \times 10^7\ M_\odot$, a few percent of the total amount of hydrogen in the disk. One must remember that other forms of $n_0(\omega)$ and $T_0(\tilde{\omega})$ could produce similar results. Nevertheless, these numerical models can be compared to two observational features: the soft X-ray background, and the mass flux of clouds falling onto the plane.

The steady-state mass flux of clouds onto one side of the plane is about $1.2\ M_\odot\ \mathrm{yr}^{-1}$ for model E2 and about $2.4\ M_\odot\ \mathrm{yr}^{-1}$ for model E1, or about the value we estimate from the observations of Oort (1970). To perform the X-ray test, full-sky X-ray maps in three intermediate-energy X-ray bands are computed for each numerical model.

iii) *X-Ray Observations*

The contribution of X-ray emission from the corona can contribute significantly to the overall brightness

of the X-ray sky for energies greater than 0.2 keV. Unfortunately, emission below 0.5 keV is partly absorbed by disk gas, so interpretation of the data is somewhat model dependent (above 0.5 keV, absorption effects are unimportant). Nevertheless, the corona should emit prodigiously below 0.5 keV (for further discussion, see Bregman 1979), so a signature of the corona would be brightening toward the galactic pole where absorption effects are smallest. In fact, brightening is clearly observed in the energy band 0.15 keV $< E <$ 0.28 keV in the northern sky for $b \gtrsim 45°$ (Sanders 1979), but a distance determination for the gas that is model independent is not yet available. Recently, Nousek (1978) attempted to disentangle the coronal emission from the total X-ray emission (disk plus halo plus background) in the 0.5–2 keV range. He removes the contribution expected from an extrapolation of the hard X-ray background, which is assumed to be extragalactic in origin. Then, using the equilibrium models of Raymond, Cox, and Smith (1977), Nousek attributes the emission to gas at two temperatures, arguing that the hotter component (3×10^6 K) has an emission measure of 3.5×10^{-3} cm^{-6} pc and lies above the neutral hydrogen of the disk. Nousek points out several uncertainties in this interpretation, such as the use of equilibrium rather than nonequilibrium plasmas. Since $\Lambda_{\rm noneq}(T) > \Lambda_{\rm eq}(T)$ if $T_{\rm electron} > T_{\rm ion}$, the temperature and emission measures Nousek calculated may be overestimates. We find that as long as $T_0 \lesssim 2.5 \times 10^6$ K, coronal X-ray emission (using equilibrium calculations of Raymond, Cox, and Smith 1976) does not violate the observational constraints. For model E1, the predicted flux is about 10^2 below the total observed flux (see Bregman 1979 for further details).

With the hope that one will someday be able to evaluate accurately the emission from the corona, we discuss the expected X-ray picture within the context of the hydrodynamic models. For three energy bands above 0.5 keV, the band cooling functions of Raymond, Cox, and Smith (1976) are approximated by a series of power laws which are given in Table 3. These approximations are used along with the hydrodynamic model to integrate the quantity

$$\mathcal{F} \equiv \int_0^\infty \Lambda n_e^2 dl$$

along a ray in a given direction. The hot coronal gas is optically thin to soft X-rays and any absorption by neutral hydrogen is neglected. Because $\mathcal{F}$ is extremely sensitive to a small reduction in T and n for $T < 2 \times 10^6$ K, only the lowest layers of corona contributes significantly to $\mathcal{F}$. Therefore, since most of the mass of the corona may not contribute to $\mathcal{F}$, it is difficult to use X-ray observations as a probe of the entire corona. At coronal temperatures greater than 2×10^6 K, most of the corona (by mass) contributes to $\mathcal{F}$, and X-ray observations are a sensitive probe to the structure of the entire corona. Since we argued above (§ IV*b*[i]) that $T_0 < 2 \times 10^6$ K is more probable than $T_0 > 2 \times 10^6$ K, only limited information about the corona can be deduced from observation.

To illustrate what we expect to observe, the X-ray band emission for model E1 is given in Table 4 as a function of galactic latitude and longitude. Note that the flux deviates from a simple csc b latitude dependence and that for fixed latitude, the flux is greater toward the galactic center than toward the anticenter. This longitude effect arises because the average electron density is about 30% higher along the ray toward $b = 30°$, $l = 0°$ than toward $b = 30°$, $l = 180°$. The degree of longitude variation of $\mathcal{F}$ is a reflection of the density and temperature gradient in the corona. Also owing to the radial gradients, $\mathcal{F}$ deviates from the simple csc b latitude dependence as seen in Table 4. The relative intensities of any two X-ray bands determines the gas temperature, and then using the band flux and derived temperature, the density and an idealized height of the gas are calculated. From the emission given in Table 4, one would infer $T_0 \approx 1 \times 10^6$ K and a density scale height of about 5 kpc [where $n(Z = 5 \text{ kpc})/n_0 = e^{-1}$). However, because $\mathcal{F}$ is very sensitive to the diminution of n and T, the X-ray scale height [h_x, where $\mathcal{F}(Z = h_x)/\mathcal{F}(Z \approx 0) = e^{-1}$] is between 1/3–1/5 of the density scale height. For the 14.2–23.3 Å band, $h_x = 1.2$ kpc, for the intermediate-energy band, $h_x = 1.4$ kpc, and for the highest-energy band, $h_x = 1.6$ kpc. Since the emission above 2 kpc

TABLE 3

APPROXIMATIONS TO THE BAND COOLING FUNCTION Λ[a]

X-Ray Band	Range of log T	α	A
14.2–23.3 Å			
(0.53–0.87 keV)...	2.70–6.23	+4.90	2.63×10^{-54}
	6.23–6.80	+0.64	8.91×10^{-28}
	6.80–7.09	−3.36	1.48
	7.09–8.00	−0.11	1.23×10^{-23}
7.95–14.2 Å			
(0.87–1.56 keV)...	2.30–6.55	+3.87	1.77×10^{-49}
	6.55–7.10	+1.22	3.85×10^{-32}
	7.10–7.42	−2.08	1.10×10^{-8}
	7.42–8.00	−0.28	4.79×10^{-22}
1.5–7.95 Å			
(1.56–8.27 keV)...	2.00–6.99	+2.847	4.79×10^{-44}
	6.99–8.00	+0.645	1.18×10^{-28}

[a] The cooling function is of the form $\Lambda = AT^\alpha$.

TABLE 4

X-RAY BRIGHTNESS ABOVE THE SUN

b (deg)	l (deg)	$\mathcal{F}$[a] (ergs cm^{-2} s^{-1}) 14.2–23.3 Å	7.95–14.2 Å	1.5–7.95 Å
30...	0	2.6×10^{-9}	1.3×10^{-10}	2.9×10^{-11}
30...	180	1.4×10^{-9}	6.8×10^{-11}	1.4×10^{-11}
60...	0	1.4×10^{-9}	7.1×10^{-11}	1.6×10^{-11}
60...	180	1.0×10^{-9}	5.3×10^{-11}	1.2×10^{-11}
90...	...	9.4×10^{-10}	4.8×10^{-11}	1.1×10^{-11}

[a] $\mathcal{F} = \int_0^\infty n_e^2 \Lambda \csc b \, dz$.

is entirely masked by emission below 2 kpc, we have no direct information about the upper corona where the clouds form.

iv) *Spiral Arms*

A real model of the Galaxy should have spiral arms in which the nature of the hot interstellar medium that enters the corona may differ greatly from the adjacent interarm region. Although we do not know observationally how n_0 and T_0 change through the spiral arm, we suspect that the increased supernova rate raises n_0, T_0, or both. This effect is tested by placing perfectly circular spiral arms in model B2; the arms are one zone wide ($\sim$0.5 kpc) and are spaced 3 kpc apart with the first one at 5 kpc. Model B2 was altered in the following three ways: (1) $2 \times n_0$, T_0 unchanged in the spiral arms; (2) $2 \times T_0$, n_0 unchanged in the arms; (3) $2 \times n_0$, $2 \times T_0$ in the arms. In each case, the enhancements of n_0 and T_0 at the arms locally raise the influx of gas into the corona. Because the pressure is higher immediately above an arm, that gas rapidly expands into the surrounding corona, and above $Z \approx$ 1–2 kpc (the mixing height), the integrity of the enhancement is lost. The mixing height of 1 kpc would be significantly reduced if the spiral arms were made narrower. The mixing height was 1.9 kpc in case 3, 1.7 kpc in case 2, and 1.1 kpc in case 1. The enhancement in n_0 and T_0 increases the mean values of coronal density and temperature. Also, the total mass of the corona is higher by $\sim$15–20% in cases (1) and (2), and about 40% in case (3) (probably an overestimate due to the unrealistic thickness of the arms). However, the presence of spiral arms does not change the radial or vertical distribution of cloud formation (i.e., the formation of clouds is not enhanced or reduced above spiral arms). Adding spiral arms to the model does not change any of the conclusions from the previous sections.

c) *Further Kinematics*

i) *Motion within the Corona*

From models D, E, and F we find that the corona does not corotate with the disk and that the angular velocity of the corona changes with both height and radius. To understand this, consider a model E corona without radiative cooling so that, eventually, the corona becomes static. On a plane at fixed Z, the rotation curve is nearly flat as a function of $\tilde{\omega}$ (as in the plane of the disk), so the angular velocity (in radians per second) decreases outward. However, each sheet has a lower rotation velocity than the one below it because $\partial\Phi/\partial\tilde{\omega}$ decreases upward while the above results are for a model without cooling. This differential motion in $\hat{Z}$ is characteristic of every numerical model. For model E1 with cooling, the rotational velocity decreases upward at the rate 13.5 km s^{-1} kpc^{-1} at $\tilde{\omega} = 15$ kpc, 10.4 km s^{-1} kpc^{-1} at $\tilde{\omega} = 12.4$ kpc, and $\sim$8 km s^{-1} kpc^{-1} at $\tilde{\omega} \leq 9$ kpc. In the frame rotating with an element of coronal gas, the radial differential velocity gradient ($\partial u_\theta/\partial\tilde{\omega}$) is 15–40 km s^{-1} kpc^{-1}, where higher values occur at low elevation and large $\tilde{\omega}$ and low values occur near the top of the corona or for small $\tilde{\omega}$. The formation of clouds occurs in a corona that has shearing motion in both $\hat{Z}$ and $\hat{\tilde{\omega}}$.

ii) *Cloud Trajectories*

Clouds return to the disk within 3–60 $\times$ 10^7 yr after formation. As viewed in a reference frame far above the disk, rotating at the angular speed of the local standard of rest, clouds appear to spiral around the disk as they fall onto it. Many clouds fail to return to their point of origin; in model E1, 30% of the clouds return to $\tilde{\omega}_i + 3$ kpc $> \tilde{\omega} > \tilde{\omega}_0 + 1$ kpc. This effect tends to make the metallicity gradient shallower than in a "closed" model (no mixing of gas between regions), and the shallower gradient is required to satisfy the observations (see Tinsley and Larsen 1978, and references therein). Because clouds do not return to their initial position, a mild circulation current is established in the disk. We also note that clouds do not penetrate the disk, because their column density (10^{19}–3 $\times$ 10^{20} cm^{-2}) is generally less than that of the disk ($\gtrsim 4 \times 10^{20}$ cm^{-2} for $\tilde{\omega} < 10$ kpc). Beyond the solar circle ($\tilde{\omega} \gtrsim 12$ kpc) the column density of disk gas is low, so clouds may penetrate the disk, though this depends on the column density of the particular cloud. Cloud collisions with the disk gas are a source of turbulent energy (in model E1, it is $\sim 3 \times 10^{40}$ ergs s^{-1} of mechanical energy, about 5% of the energy supplied by supernovae).

iii) *Predicted Map of Clouds on the Sky*

In addition to the general prediction that the velocities of the IVC/HVC are reproduced as clouds that fall from their initial position (§ IV*a*), we can statistically predict their velocity distribution on the sky. To do this, we neglect ram pressure and assume that clouds form randomly throughout the corona. For model E1, an all-sky distribution is presented in Figure 5. As the density is decreased (e.g., from model E1 to E3), the number of positive IVC/HVC decreases between 60° and 300° because fewer clouds form with positive radial velocity (i.e., the corona becomes more nearly static in $\tilde{\omega}$ as n_0 decreases, so that $t_{\rm cool}$ becomes much longer than $t_{\rm eq}$ and the flow velocity at which clouds form is very small). The percentage of negative IVC/HVC between 60° and 300° increases as the temperature is increased, as does the percentage of positive clouds between $-60°$ and 60°. Clearly, gross velocity features of the IVC/HVC are reproduced in Figure 5. However, one should not hope that Figure 5 will reproduce the detailed cloud distribution because the formation of individual clouds is not random (as assumed)—they form in coherent patterns (see § IV*a*).

iv) *Cloud Drag and Pressure Confinement*

In addition to the previously discussed physical and observational conditions which our model satisfies, we also show that the clouds indeed fall ballistically, and that they are approximately in pressure equilibrium with the corona after formation. The cloud

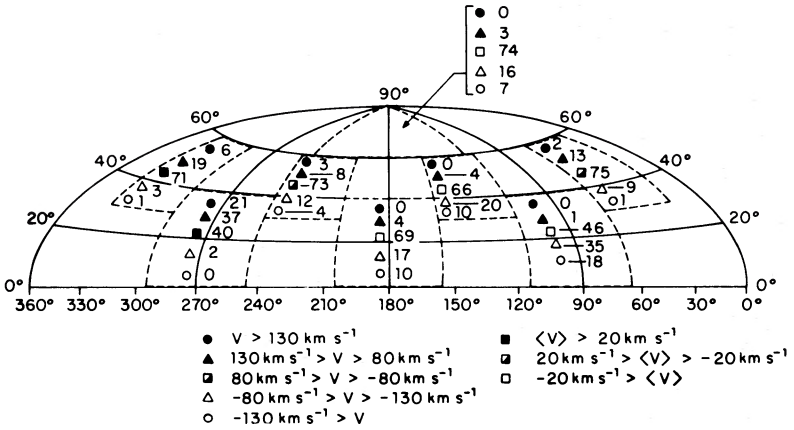

FIG. 5.—Distribution of IVC/HVC on the sky is theoretically predicted. Within each region delineated by dotted lines, the relative percentages of clouds is listed next to their velocity range (for a total of 100% in each region). Each zone centered at $b = 20°$ is 50° wide; zones with $30° < b < 60°$ are 40° wide, and the zone that reaches to $b = 90°$ is 120° wide. Note that many clouds have low velocities and will be confused with normal disk gas.

trajectories calculated above are valid only if the gravitational force is much greater than drag force experienced by the cloud passing through the corona. Stated another way, the terminal velocity at which gravitational and drag forces balance must be somewhat greater than their observed velocities if drag is to be neglected. When we use the Newtonian approximation to calculate the drag on a spherical cloud, the terminal velocity is

$$V_t = 370\left(\frac{n_{\rm cl}L_{\rm cl}}{10^{20}\ {\rm cm}^{-2}}\right)^{1/2}\left(\frac{n}{10^{-3}\ {\rm cm}^{-3}}\right)^{-1/2} \times \left(\frac{g}{10^{-8}\ {\rm cm\ s}^{-2}}\right)^{1/2} {\rm km\ s}^{-1},$$

where $n_{\rm cl}L_{\rm cl}$ is the column density of a cloud. Most clouds on the list of Hulsbosch (1975) have a column density greater than 5×10^{19} cm^{-2} ($V_t \gtrsim 260$ km s^{-1}) and since the drag force is proportional to velocity squared, drag is generally a small effect. However, a few of the lowest column density clouds listed by Hulsbosch (1975) appear to be traveling near their terminal velocity (cloud $119.5+10.5$ has $V = -160$ km s^{-1}, $nL = 2 \times 10^{19}$ cm^{-2}, and $|V_t| \approx 165$ km s^{-1}; $90+35$ has $V = -165$ km s^{-1}, $nL = 2 \times 10^{19}$ cm^{-2}, and $|V_t| = 165$ km s^{-1}; $161+146$ has $v = -167$ km s^{-1}, $nL = 3 \times 10^{19}$ cm^{-2}, and $|V_t| = 202$ km s^{-1}). Drag will preferentially compress one face of a cloud.

The pressure in the corona (2000 K cm$^{-3} > P/k > 400$ K cm^{-3}) is balanced by the thermal and magnetic pressure in the clouds (the clouds are not gravitationally bound). If the cloud temperature is several hundred degrees (Payne *et al.* 1978), then $n \approx 1$–10 cm^{-3} if magnetic pressure is negligible. From the work of Hulsbosch (1975), who models the observed clouds with a spherical, Gaussian density distribution, we infer that the average density is $n \approx 0.7$ cm^{-3}. In these cold clouds, magnetic pressure may be important, and a modest field of several microgauss will balance the thermal pressure of the corona. Therefore, either the coronal pressure lies toward the low end of the permissible regime and is balanced by thermal cloud pressure, or magnetic pressure is important in the cloud.

V. ROLE OF MAGNETIC FIELDS

The strength and alignment of magnetic fields control the rate of thermal conduction and the magnitude of the magnetic pressure, which can be important terms in the energy equation and momentum equation, respectively. Only if no magnetic field exists, or if the field lines are not tangled and not perpendicular to the temperature gradient, can electron conduction be significant; in a hydrostatic atmosphere, conduction is of major importance in the overall structure of the corona when

$$\nabla\cdot\boldsymbol{q} \geq n^2\Lambda\,, \qquad (5.1)$$

where $\boldsymbol{q}$ is the heat flux vector. We approximate $\nabla\cdot\boldsymbol{q}$ as $\kappa T/L^2$, where the coefficient of conductivity is (Spitzer 1962) $\kappa = 1.84 \times 10^{-5}(T^{5/2}/\ln\Lambda')$ and L is the temperature length scale in the corona. With the cooling function $\Lambda = 6.2 \times 10^{-19}T^{-0.6}$ ergs cm^2 s^{-1} (McKee and Cowie 1977), and the substitution of $L = S$ (from eq. [4.9b]) we find that conduction is important when

$$\left(\frac{g}{10^{-8}\ {\rm cm\ s}^{-2}}\right)\left(\frac{n}{10^{-3}\ {\rm cm}^{-3}}\right)^{-1}\left(\frac{T}{10^6\ {\rm K}}\right) \gtrsim 10\,. \qquad (5.2)$$

So, unless the corona is of low density ($n_{-3} \lesssim 0.1$), the overall structure of the corona is virtually unchanged. This argument is substantiated by numerical models with conduction (see Bregman 1978 for a description of the numerical procedure).

While the large-scale structure is unchanged, conduction can suppress the formation of small clouds.

The minimum wavelength below which condensations do not occur is (Field 1965; Mathews and Bregman 1978; Chevalier and Oegerle 1979; perfect conductive efficiency)

$$\lambda \approx 2\left(\frac{T}{10^6\ \mathrm{K}}\right)^2\left(\frac{n}{1\times 10^{-3}\ \mathrm{cm}^{-3}}\right)^{-1}\ \mathrm{kpc}\,. \quad (5.3)$$

This implies that only large regions initially more massive than

$$M \approx 1\times 10^5\left(\frac{T}{10^6\ \mathrm{K}}\right)^6\left(\frac{n}{1\times 10^{-3}}\right)^{-2} M_\odot \quad (5.4)$$

can begin to form a cloud. As large, thermally unstable regions cool, T and λ decrease so that smaller condensations may develop within it. This process continues until the temperature falls below the thermally unstable region (below 2×10^5 K), after which no more subcondensations form. So when the temperature falls into the range $2\times 10^5\ \mathrm{K} \lesssim T \lesssim 4\times 10^5$ K, the growth of condensations ceases. Since the mass of condensation in pressure equilibrium with its surroundings is proportional to T^8 (from eq. [5.3]), we estimate that the smallest condensation will be of 10^2–$10^{-0.5}\ M_\odot$ (for $2\times 10^5\ \mathrm{K} \lesssim T \lesssim 4\times 10^5$ K; growth of the $10^{-0.5}\ M_\odot$ clouds, which begin to form when $T \approx 2\times 10^5\ M_\odot$, will probably be damped when T falls below 10^5 K). Hulsbosch (1975) estimates masses for the HVC as low as $10^2\ M_\odot$ which is consistent with, but not proof of, the above argument. Alternatively, if subcondensations never occur, then in order to explain the formation of small HVC, electron conduction must be at least 10–10^2 less efficient than the optimum conditions. This occurs if magnetic fields are tangled on a scale length smaller than the clouds.

Tangled magnetic fields resist compression by exerting a pressure of $B^2/8\pi$. Magnetic pressure stops cloud condensation if it is greater than the gas pressure. To estimate the relative pressure, we assume that $B \propto n^{2/3}$, and that $B = 4\times 10^{-6}$ gauss, $n = 0.1\ \mathrm{cm}^{-3}$ in the intercloud medium of the disk (Heiles 1976); in the corona we find that

$$P_{\mathrm{gas}}/P_B = 200\times\left(\frac{n}{1\times 10^{-3}}\right)^{-1/3}\left(\frac{T}{10^6\ \mathrm{K}}\right) > 1\,.$$

Therefore, unless B can be generated within the corona, magnetic pressure is not globally important.

Nonuniform rotation and internal turbulence (cyclonic convection) in the corona will generate magnetic fields (the galactic dynamo; Parker 1971*a*, *b*, Stix 1975) if the growth time for dynamo modes is shorter than the lifetime of gas in the corona ($\lesssim 10^8$ yr, models E). We estimate the growth time in the most easily excited mode, the quadrupolar mode, by letting the turbulent velocity be the sound speed and letting the eddy size be the scale height. This crude calculation indicates a growth time of $\sim 10^8$ yr (about the same value that Parker 1971*a* estimates for the disk gas), so it may be possible for the corona to act as a dynamo.

VI. DISCUSSION

a) Chains of High-Velocity Clouds

There are several distinct groupings or "streams" of HVC in the sky—clouds are not always randomly placed. In the context of our model, this indicates that the perturbations which trigger thermal instabilities are coherent on a scale of about a kiloparsec; we mention three ways this occurs. (1) The Magellanic Clouds exerted a strong influence on the corona as it passed, and it still tidally influences the corona, although weakly. Consequently, these tidal effects produce a coherent perturbation in the corona. (2) As hot gas rises from the disk, it drags magnetic field lines with it; since the magnetic field lines are still connected to the disk, a neutral sheet develops behind the rising gas. Although the magnetic pressure is small compared to the total pressure, the neutral sheet (zero magnetic field) causes a perturbation in the gas pressure which is coherent over a long scale length. As Field (1965) pointed out, a perturbation in the magnetic field can trigger a thermal instability. (3) If conduction is fairly efficient, then only large perturbations are thermally unstable (§ V), and as discussed in § V, smaller clouds develop in the large perturbation and an association of clouds naturally results.

Differential rotation in the corona acts to deform the initial shape of these large groupings of clouds. Shear, primarily from $\partial(\bar{\omega}u_\theta)/\partial\bar{\omega}$, but also from du_θ/dZ, stretches out the groups of clouds in θ so that it covers a wide angular extent in the sky while remaining narrow in the other two dimensions. The shearing begins when a density perturbation forms into a cloud, during which time a spherical perturbation develops an axial ratio of 2:1 in model E1 and 4:1 in model E3 (the higher axial ratio is due to the longer formation time). The shearing continues until the clouds intercept the plane, when the axial ratio grows to 3:1–15:1, depending upon where the clouds form. As seen in Figure 4, initial perturbations are probably narrow in Z compared to their extent in $\bar{\omega}$ and θ; they are not spherical as assumed in the above discussion. This flatness of perturbations will amplify the apparent axial ratio of cloud groups that intercept the plane beyond the Sun. Another earmark of cloud formation via thermal instabilities is that clouds have dense irregularities as large as or larger than a parsec, the size of the smallest subcondensation that can form.

So within the context of the models described in § IV, streams of HVC arise because coherent perturbations stimulate the formation of groups of clouds, and differential rotation stretches them out in θ.

b) Stripping Globular Cluster Gas

The coronal gas can play an important role in stripping gas from globular clusters. For the maximum possible coronal density, we apply the calculations of Frank and Gisler (1976) and find that about half the globular clusters are initially stripped of gas. In the most tightly bound clusters, other gas removal mechanisms, such as winds, are necessary to initially

remove the gas (Scott and Rose 1975; VandenBerg and Faulkner 1977; VandenBerg 1978). Once clusters are gas-free, they remain so either by continuous stripping (which differs from initial stripping: Bregman 1978) or by winds.

c) *Other Relevant Observations*

Savage and de Boer (1979) have recently obtained high resolution UV spectra of two hot stars in the Large Magellanic Clouds ($l \sim 280°$, $b \sim 32°$). They report the presence of very strong and asymmetrical lines of C IV and Si IV (wings extend to $+120$ km s^{-1}) and strong absorption lines of C II, O I, N I, Si II, and Al II with asymmetric wings extending to $V_{\rm LSR} \approx +140$ km s^{-1}. The blueshift is attributed to normal differential galactic rotation of a corotating corona, and by using the Schmidt (1965) model they place the gas at $\tilde{\omega} \sim 15$ kpc, $Z \sim 8$ kpc. When more recent models of galactic rotation are used (Innanen 1973, or flat rotation curve), the distance of the absorbing gas becomes $\tilde{\omega} \sim 18$–30 kpc. However, if the absorbing gas is part of the galactic fountain, differential rotation is amplified (§ II*b*, model *a*), and even with current models of galactic rotation, the absorbing gas is at $\tilde{\omega} \approx 15$ kpc. The coronal temperature and density at $\tilde{\omega} \approx 15$ kpc, $Z \approx 5$ kpc (model E1) are about 6×10^5 K and 2×10^{-4} cm^{-3}; this position is slightly below the cloud-forming region. Savage and de Boer (1979) estimate the density and temperature to be 3×10^{-4} cm^{-3} and 10^5 K, respectively. We suggest that the absorbing material is coronal gas that has begun to cool into what will eventually be recognized as cold neutral clouds.

d) *Future Work*

Galactic coronae may be common in gas-rich spiral galaxies. This suggestion can be observationally tested by observing edge-on spiral galaxies in the 0.5–4 keV regime. An emitting region up to several kiloparsecs thick should be visible.

Throughout this work, the local explanation for the IVC/HVC (Siluk and Silk 1974; Weaver 1978) has been ignored because the existing distance estimates imply that the clouds are above the disk (§ II*a*). The distance determinations for the clouds desperately need to be improved before one can decisively choose between the local and the external model.

I am grateful to the Goddard Institute for Space Studies for use of their computer facilities. For comments, advice, and information, I thank E. Scharlemann, E. Spiegel, F. Shu, C. McKee, J.H. Oort, R. Giovanelli, and a number of others. Also, S. Baker and S. Mescher were especially helpful in preparing the manuscript. The interpretative representation of the galactic corona (Fig. 1) was rendered by Donna Diamond. This work was supported by NSF grants AST 77-07841 and AST 76-08917.

REFERENCES

Blitz, L. 1979, private communication.
Bregman, J. N. 1978, *Ap. J.*, **224**, 768.
———. 1979, *Ap. J.*, **229**, 514.
Chevalier, R. A., and Gardner, J. 1974, *Ap. J.*, **192**, 457.
Chevalier, R. A., and Oegerle, W. R. 1979, *Ap. J.*, **227**, 398.
Cox, D. P. 1972, *Ap. J.*, **178**, 159.
Davies, R. D. 1972*a*, *Nature*, **273**, 88.
———. 1972*b*, *M.N.R.A.S.*, **160**, 381.
———. 1975, in *IAU Symposium No. 40, Galactic Radio Astronomy*, ed. F. J. Kerr and S. C. Simonson III (Dordrecht: Reidel), p. 599.
de Vaucouleurs, G. 1978, in *IAU Symposium No. 84, The Large-Scale Characteristics of the Galaxy*, ed. W. B. Burton (Dordrecht: Reidel), in press.
Field, G. B. 1965, *Ap. J.*, **142**, 531.
———. 1975*a*, *Ap. Space Sci.*, **38**, 167.
———. 1975*b*, in *Atomic and Molecular Physics of the Interstellar Medium*, ed. R. Balian, P. Encrenaz, and J. Lequeux (Amsterdam: North-Holland), p. 467.
Field, G. B., and Perrenod, S. C. 1977, *Ap. J.*, **215**, 717.
Frank, J., and Gisler, G. 1976, *M.N.R.A.S.*, **176**, 533.
Giovanelli, R. 1978, in *IAU Symposium No. 84, The Large-Scale Characteristics of the Galaxy*, ed. W. B. Burton (Dordrecht: Reidel), in press.
Giovanelli, R., and Haynes, M. P. 1976, *M.N.R.A.S.*, **177**, 525.
Gordon, M. A., and Burton, W. B. 1976, *Ap. J.*, **208**, 346.
Habing, H. J. 1966, *Bull. Astr. Inst. Netherlands*, **18**, 323.
Heiles, C. 1976, *Ann. Rev. Astr. Ap.*, **14**, 1.
Hulsbosch, A. N. M. 1968, *Bull. Astr. Inst. Netherlands*, **20**, 33.
———. 1975, *Astr. Ap.*, **40**, 1.
———. 1978, *Astr. Ap.*, **66**, L5.
Hulsbosch, A. N. M., and Oort, J. H. 1973, *Astr. Ap.*, **22**, 153.
Hulsbosch, A. N. M., and Raimond, E. 1966, *Bull. Astr. Inst. Netherlands*, **18**, 413.
Innanen, K. A. 1973, *Ap. Space Sci.*, **22**, 393.
Jackson, P. D., Fitzgerald, M. P., and Moffat, A. F. J. 1978, in *IAU Symposium No. 84, The Large-Scale Characteristics of the Galaxy*, ed. W. B. Burton (Dordrecht: Reidel), in press.
Jenkins, E. B. 1978, *Ap. J.*, **220**, 107.
Krumm, N., and Salpeter, E. E. 1976, *Ap. J.* (*Letters*), **208**, L7.
Mathews, W. G., and Bregman, J. N. 1978, *Ap. J.*, **224**, 308.
McKee, C. F., and Cowie, L. L. 1977, *Ap. J.*, **215**, 213.
McKee, C. F., and Ostriker, J. P. 1977, *Ap. J.*, **211**, 148.
Muller, C. A., Raimond, E., Schwarz, U. J., and Tolbert, C. R. 1966, *Bull. Astr. Inst. Netherlands Suppl.*, **1**, 213.
Nousek, J. 1978, Ph.D. thesis, University of Wisconsin at Madison.
Oort, J. H. 1966, *Bull. Astr. Inst. Netherlands*, **18**, 421.
———. 1967, in *IAU Symposium No. 31, Radio Astronomy and the Galactic System*, ed. H. van Woerden (New York: Academic Press), p. 279.
———. 1969, *Nature*, **224**, 1158.
———. 1970, *Astr. Ap.*, **7**, 381.
———. 1978, preprint.
———. 1979, private communication.
Oort, J. H., and Hulsbosch, A. N. M. 1978, in *Astronomical Papers Dedicated to Bent Strömgren*, ed. A. Reiz (Copenhagen: Copenhagen University Observatory), p. 409.
Oort, J. H., and Plaut, L. 1975, *Astr. Ap.*, **41**, 71.
Ostriker, J. P. 1978, in *IAU Symposium No. 84, The Large-Scale Characteristics of the Galaxy*, ed. W. B. Burton (Dordrecht: Reidel), in press.
Parker, E. N. 1971*a*, *Ap. J.*, **163**, 255.
———. 1971*b*, *Ap. J.*, **164**, 491.
Payne, H. E., Dickey, J. M., Salpeter, E. E., and Terzian, Y. 1978, *Ap. J.* (*Letters*), **221**, L95.
Raymond, J. C., Cox, D. P., and Smith, B. W. 1976, *Ap. J.*, **204**, 290.
Rickard, J. J. 1971, *Astr. Ap.*, **11**, 270.

Rubin, V. C. 1978, in *IAU Symposium No. 84, The Large-Scale Characteristics of the Galaxy*, ed. W. B. Burton (Dordrecht: Reidel), in press.
Sanders, W. T. 1979, private communication.
Sanders, W. T., Kraushaar, W. L., Nousek, J. A., and Fried, P. M. 1977, *Ap. J. (Letters)*, **217**, L87.
Savage, B. D., and de Boer, K. S. 1979, *Ap. J. (Letters)*, **230**, L77.
Schmidt, M. 1956, *Bull. Astr. Inst. Netherlands*, **13**, 15.
———. 1965, *Stars and Stellar Systems*, Vol. **5**, ed. A. Blaauw and M. Schmidt (Chicago: University of Chicago Press), p.513.
Scott, E. H., and Rose, W. K. 1975, *Ap. J.*, **197**, 147.
Shapiro, P. R., and Field, G. B. 1976, *Ap. J.*, **205**, 762.
Shapiro, P. R., and Moore, R. T. 1976, *Ap. J.*, **207**, 406.
Silk, J. 1974, *Comments Ap. Space Sci.*, **6**, 1.
Siluk, R. S., and Silk, J. 1974, *Ap. J.*, **192**, 51.
Spitzer, L. 1956, *Ap. J.*, **124**, 20.
———. 1962, *Physics of Fully Ionized Gasses* (New York: Interscience).
Stix, M. 1975, *Astr. Ap.*, **42**, 85.
Tammann, G. A. 1977, European Southern Obs. Sci. preprint, No. 4.
Tinsley, B. M., and Larson, R. B. 1978, *Ap. J.*, **221**, 554.
VandenBerg, D. A. 1978, *Ap. J.*, **224**, 394.
VandenBerg, D. A., and Faulkner, D. J. 1977, *Ap. J.*, **218**, 415.
Verschuur, G. L. 1973, *Astr. Ap.*, **22**, 139.
———. 1975, *Ann. Rev. Astr. Ap.*, **13**, 257.
Wannier, P., Wrixon, G. T., and Wilson, R. W. 1972, *Astr. Ap.*, **18**, 224.
Waxman, A. M. 1978, *Ap. J.*, **222**, 61.
Weaver, H. 1978, in *IAU Symposium No. 84, The Large-Scale Characteristics of the Galaxy*, ed. W. B. Burton (Dordrecht: Reidel), in press.
Weisheit, J. C., and Collins, L. A. 1976, *Ap. J.*, **210**, 299.
Williamson, F. O., Sanders, W. T., Kraushaar, W. L., McCammon, D., Borken, R., and Bunner, A. N. 1974, *Ap. J. (Letters)*, **193**, L133.

JOEL N. BREGMAN: Columbia University, Department of Astronomy, New York, NY 10027